

Investigating observability properties from data in nonlinear dynamics

Luis A. Aguirre¹ and Christophe Letellier²¹*Departamento de Engenharia Eletrônica, Universidade Federal de Minas Gerais, Avenida Antônio Carlos 6627, 31270-901 Belo Horizonte MG, Brazil*²*CORIA UMR 6614, Université de Rouen, Avenue de l'Université, BP 12, F-76801 Saint-Etienne du Rouvray Cedex, France*

(Received 10 February 2011; published 22 June 2011)

Investigation of observability properties of nonlinear dynamical systems aims at giving a hint on how much dynamical information can be retrieved from a system using a certain measuring function. Such an investigation usually requires knowledge of the system equations. This paper addresses the challenging problem of investigating observability properties of a system only from recorded data. From previous studies it is known that phase spaces reconstructed from poor observables are characterized by local sharp pleatings, local strong squeezing of trajectories, and global inhomogeneity. A statistic is then proposed to quantify such properties of poor observability. Such a statistic was computed for a number of bench models for which observability studies had been previously performed. It was found that the statistic proposed in this paper, estimated exclusively from data, correlates generally well with observability results obtained using the system equations. It is possible to arrive at the same order of observability among the state variables using the proposed statistic even in the presence of noise with a standard deviation as high as 10% of the data. The paper includes the application of the proposed statistic to sunspot time series.

DOI: [10.1103/PhysRevE.83.066209](https://doi.org/10.1103/PhysRevE.83.066209)

PACS number(s): 05.45.Tp

I. INTRODUCTION

Consider a system $\dot{\mathbf{x}} = \mathbf{f}(\mathbf{x})$ from which only a scalar variable $s(t)$ is recorded according to a measurement function $h: s(t) = h(\mathbf{x})$. A key problem in nonlinear dynamics is to reconstruct a phase space from $s(t)$ that will convey dynamical information from the unknown original phase space. Suppose $\mathbf{x} \in \mathbb{R}^m$, roughly speaking, the observability problem in control engineering is to determine if it is possible to recover (observe) \mathbf{x} from $s(t)$ and a model of the dynamics (the observer). A different but somewhat related problem in the embedding of nonlinear dynamics is to establish a d -dimensional set of coordinates from $s(t)$ in such a way that the reconstructed space can be used as a working space where geometrical and dynamical features of the system can be assessed. In a typical embedding problem there is no need to recover the state vector \mathbf{x} and, unlike the observability problem in the context of control engineering, the embedding dimension is usually different from the original phase space dimension, that is, $d \neq m$.

One of the similarities of the aforementioned approaches to observability is the need of system equations [1,2]. The aim of the present paper is to investigate the observability problem, in the context of nonlinear dynamics, only from data. Since the definition of observability is based on the system equations [3], in order to address the problem from data, we use previous knowledge on some of the main features of phase spaces reconstructed from poor and good observables. Having established such features, the paper proceeds to define a statistic which is able to quantify such features from data. The results are compared to observability results known from the theory to see how the new statistic correlates with such knowledge. Smirnov and colleagues have investigated an observability-related problem in the context of modeling [4].

In particular, it is assumed that a good embedding will be approximately linear in any small neighborhood in phase space. Poor embeddings, as, for instance, those obtained

using variables that provide poor observability of the original dynamics, are characterized by strong pleatings and trajectory squeezing in the reconstructed space. In this paper a “pleat” will be distinguished from a “fold.” A *fold* is associated with a topological structure that molds the dynamics and which cannot be removed, no matter in which space the phase portrait is reconstructed. Contrary to this, a *pleat* is a spurious structure without any dynamical role and which does not exist in the original phase space. The existence of a pleat depends on the measurement function and, consequently, the reconstructed space in which the dynamics is investigated. These “nonlinear features” are not related to the dynamics but rather to projection side effects of the measurement function h . Typically, provided the neighborhood is sufficiently small, foldings still correspond to a locally linear structure, since the dynamics results from a set of smooth differential equations. Most of the spurious features are detected by noticing that, locally in the reconstructed space, there will be some departure from linearity, and such a departure can be quantified by a decrease in relative importance of the main linear components. A key tool is the application of a singular value decomposition to a matrix composed of trajectory segments contained in a “small” neighborhood.

A pioneering work in the use of the singular value decomposition (SVD) in the field of nonlinear signal processing is Ref. [5]. In that paper the SVD was proposed as a way of providing a set of coordinates that are alternatives to the *differential* and *delay* coordinates [6,7] and to determine an adequate value for the embedding dimension. More recent studies on the SVD and embedding techniques include Refs. [8] and [9]. SVD only takes into account linear structures [10]. Although a nonlinear extension of the SVD seems to be possible [11], in this paper, however, the SVD is only applied locally. The aim is simply to assess the local deviation from linearity by applying the SVD to rather small neighborhoods in the reconstruction space. In this case typical difficulties due to nonlinearity are avoided [12].

The important problem of the noise floor is of little relevance for the method proposed in this paper because what is assessed is the local simplicity of the embedding. In order to do so, we use a statistic [see Eq. (6)], where no decision on the statistical significance of singular values is required. The rationale behind our investigation is that good embeddings will, in practice, be “locally simple” and globally homogeneous. Poor embeddings, on the other hand, reveal locally a more complex structure due to pleating and squeezing. In other words, good embeddings deviate less from a locally linear manifold than do poor embeddings. The statistic defined in this paper [see Eq. (6) below] quantifies the relative importance of one (linear) direction explaining the reconstructed data. If the embedding is poor, for whatever reason, the relative importance of the best—in a SVD sense—(linear) direction will decrease.

A somewhat related reasoning was used in Ref. [13] where a measure of the average local deformation was defined based on the growth rate of the error vector between a reference point and the center of mass of the neighborhood. In that paper the authors’ main assumption was that “in a bad reconstruction adjacent trajectories may have very different directions” [13], p. 7079]. Such local applications of the SVD date back to Ref. [14] and have been applied even

to nonlinear dynamics (topological dimension estimation) in Ref. [12].

The paper is organized as follows. Background material is provided in Sec. II. The main result of the paper is given in Sec. III, and numerical examples are provided in Sec. IV. The main conclusions of the paper are discussed in Sec. V.

II. BACKGROUND

Consider a nonlinear system

$$\begin{aligned} \dot{\mathbf{x}} &= \mathbf{f}(\mathbf{x}), \\ s(t) &= h(\mathbf{x}), \end{aligned} \tag{1}$$

with $\mathbf{f} : \mathbb{R}^m \rightarrow \mathbb{R}^m$ and $h : \mathbb{R}^m \rightarrow \mathbb{R}$. A vector in a differential embedding space of dimension d is

$$s^T(t) = [s(t) \dot{s}(t) \ddot{s}(t) \cdots s^{(d-1)}(t)], \tag{2}$$

where $s^{(d-1)}(t)$ indicates $d^{(d-1)}s(t)/dt^{(d-1)}$, and a vector in a delay embedding space of dimension d is

$$s_k^T = [s(k) s(k + \tau) s(k + 2\tau) \cdots s(k + (d - 1)\tau)], \tag{3}$$

where $s(k)$ is the k th recording of $s(t)$ sampled with sampling interval T_s , and τ is a delay time. A *trajectory matrix* can be defined as

$$X = \begin{bmatrix} s_k^T \\ s_{k+\tau}^T \\ \vdots \\ s_{k+(N-1)\tau}^T \end{bmatrix} = \begin{bmatrix} s(k) & s(k + \tau) & \cdots & s(k + (d - 1)\tau) \\ s(k + \tau) & s(k + 2\tau) & \cdots & s(k + d\tau) \\ \vdots & \vdots & \ddots & \vdots \\ s(k + (N - 1)\tau) & s(k + N\tau) & \cdots & s(k + (N + d - 2)\tau) \end{bmatrix}. \tag{4}$$

The trajectory matrix $X \in \mathbb{R}^{N \times d}, N > d$ can be decomposed using the SVD as [5]

$$X = S \Sigma C^T, \tag{5}$$

where S and C are orthogonal matrices and Σ is a diagonal matrix of singular values of X , that is, $\Sigma = \text{diag}[\sigma_1, \dots, \sigma_d]$, where it is assumed that $\sigma_1 > \sigma_2 > \cdots > \sigma_d$. Let us further assume that the data in the original phase space \mathbf{x} are on a manifold of dimension $n < m$. For a generic measuring function h there will be a diffeomorphism between the original and embedding spaces if $d \geq 2n + 1$ [7]. The vectors that compose matrix C can be used as the coordinates of yet another embedding space. Moreover, if only $d' < d$ singular values are greater than zero—or greater than the noise floor in the case of noisy data—the first d' vectors in C can be used as a set of coordinates for an embedding space of reduced dimension d' [5].

III. LOCAL MEASURES OF SIMPLICITY AND OBSERVABILITY

One of the main features of a good reconstruction space is that the dynamics should be adequately unpleated in it. For instance, it is well known that if the delay time is too small, the

data are squeezed along the main diagonal of the reconstructed space using delay coordinates.

We shall return to delay coordinates later, but for now let us consider differential embeddings. It is also known that, depending on the measuring function h , the reconstructed space $[s \dot{s} \ddot{s} \cdots s^{(d-1)}]$ might not be an embedding [15]. Careful investigation of this problem reveals that when the recorded variable is a poor observable, it is usually possible to find in the reconstructed space regions, where the trajectories are either squeezed or they are strongly pleated. In such regions there is no (local) diffeomorphism relating the original and reconstructed spaces, therefore, it is not possible to know the original dynamics from the reconstructed space in that particular region. Such a scenario is the result of a choice of observable that renders poor observability of the system. On the other hand, in a favorable scenario, the dynamics are comfortably unpleated throughout the reconstructed space.

The main idea in this paper is to be able to quantify the *local* “unpleatedness” of the dynamics. If the dynamics are well unpleated in a neighborhood \mathcal{U} , the geometry in \mathcal{U} is simple, and this is indicated by a relatively large first singular value of a trajectory matrix build with data taken from the neighborhood \mathcal{U} . Conversely, when the data are pleated in the reconstruction

space, the local structure becomes more complicated and the subsequent, i.e., second, third, etc., singular values become relatively more important. Therefore, a simple indication of the geometrical simplicity of the dynamics within \mathcal{U} is given by

$$\sigma_{1\%}(\mathcal{U}) = \frac{\sigma_1}{\text{Tr}[\Sigma]} 100, \quad (6)$$

where $\text{Tr}[\Sigma]$ indicates the trace of matrix Σ , that is, the summation of all the singular values $\sigma_i, i = 1, \dots, d$ and $\sigma_{1\%}(\mathcal{U})$ is a relative measure of the largest singular value of a matrix with data taken from the neighborhood \mathcal{U} . Therefore, large values of $\sigma_{1\%}$ indicate the lack of sharp pleatings, which is expected if the dynamics is comfortably unpleated. Conversely, as the system visits regions in reconstructed space where the dynamics is more strongly pleated, $\sigma_{1\%}$ decreases. From a reconstruction point of view, the larger $\sigma_{1\%}$, the better. Hence, if the reconstructed space presents pleating, e.g., due to a bad observable, it will depart from local linearity and this will be detected by a reduction in the relative importance of the first singular value. It is important to see that the neighborhoods need not (and should not) be too small, in order to help detect the departure from linearity.

Therefore, a good embedding is obtained whenever the dynamics is unpleated in the reconstruction space in an homogeneous way. Conversely, whenever the dynamics is unpleated in a nonhomogeneous way, the resulting embedding is poor, that is, there are regions of the reconstructed space that have a very simple geometry, and there are other regions that display a more complicated structure. Since we propose to use $\sigma_{1\%}$ as a local measure of the geometrical simplicity of the reconstructed space, then the overall features of the reconstructed space can be quantified by some measure of the variability of $\sigma_{1\%}$ throughout the space.

In a sense this method is similar to the one proposed in Ref. [16], where a measure of homogeneity of the flow was calculated. However, in that paper the authors developed a quantitative measure of the violation of causality that consists of following the evolution of the distance between two neighboring points.

In this paper we propose to follow a simple yet effective procedure. First, we take a time series of the observable s and embed it in the reconstruction space using some coordinate system. A certain number of neighborhoods that are located all over the reconstructed space is chosen and for each such neighborhoods $\sigma_{1\%}$ is calculated. Finally, we simply compute the statistic

$$S_s = \frac{\text{mean}[\sigma_{1\%}(\mathcal{U})]}{100 \text{std}[\sigma_{1\%}(\mathcal{U})]}, \quad (7)$$

where ‘‘mean’’ stands for the sample mean and ‘‘std’’ is the sample standard deviation of $\sigma_{1\%}$ over the population of neighborhoods \mathcal{U} . The idea behind (7) is that a reconstructed space for which $\sigma_{1\%}$ is larger on average will indicate better unpleating of the dynamics. Also, smaller variability, that is smaller $\text{std}(\sigma_{1\%})$, will indicate a more homogeneous reconstructed space, which is also the signature of a reconstruction based on a good observable.

The details as to how to compute (6) are give below. Let $s_1, s_2 \in \mathbb{R}^d$ be two vectors in the reconstructed space \mathbb{R}^d . These

vectors are neighbors within a tolerance ϵ if $|s_1 - s_2| < \epsilon$, where $|\cdot|$ indicates some norm. In this paper the L_1 norm was used. A neighborhood \mathcal{U} can be defined by taking some reference vector $s_r \in \mathbb{R}^d$ and searching for all the vectors in the data that satisfy $|s_r - s_i| < \epsilon, \forall i$. Suppose that for a given reference s_r the vectors $s_i, i = j_1, j_2, \dots, j_N$ were found to be neighbors with neighborhood size defined by ϵ . Let us denote such a neighborhood by \mathcal{U} . The (local) data matrix for neighborhood \mathcal{U} is formed thus,

$$X_{\mathcal{U}}(s_r, \epsilon) = \begin{bmatrix} s_{j_1}^T \\ s_{j_2}^T \\ \vdots \\ s_{j_N}^T \end{bmatrix}. \quad (8)$$

In what follows, the arguments of $X_{\mathcal{U}}(s_r, \epsilon)$ will be omitted for the sake of simplicity. The singular value decomposition of the local data matrix is given as before [see Eq. (5)],

$$X_{\mathcal{U}} = S \Sigma C^T, \quad (9)$$

and the elements of Σ are used directly in (6).

The use of Eq. (7), as will be seen, is particularly relevant in observability problems where poor observables usually result in *local* blind spots in the reconstructed space. Such blind spots are usually characterized by sharp pleatings and/or strong squeezing of trajectories and therefore they locally deviate from linear manifolds. Such a deviation is captured by the singular value decomposition observability (SVDO) statistic, S_s . In Secs. III A and IV the statistic in (7) will be computed for a number of cases for which the observability features of the variables are known. Thus the practical use of (7) in assessing observability features directly from data can be established.

A. A benchmark example

To illustrate, consider the Rössler system [17],

$$\begin{aligned} \dot{x} &= -y - z, \\ \dot{y} &= x + ay, \\ \dot{z} &= b + z(x - c), \end{aligned} \quad (10)$$

with $(a, b, c) = (0.398, 2.0, 4.0)$. This has become a benchmark example in what concerns observability, because, in a sense, it provides two extremes: On the one hand, the phase space reconstructed with (y, \dot{y}, \ddot{y}) is globally diffeomorphic to the original phase space. On the other hand, the z variable is known to be a particularly poor observable for this system [18,19]. Various ways of computing the degree of observability yield the same ranking among the variables, $y \triangleright x \triangleright z$, which can be considered the correct one for this simple system, where $y \triangleright x$ means that y is a better observable than x , and so on.

System (10) was simulated from random initial conditions, with an integration step equal to 0.01 for a final time of $t = 300$. The first part of the simulated trajectory was discarded to avoid any spurious effects due to transients. In order to establish the main features of the proposed procedure free of any numerical artifacts, the first and second time derivatives of the state variables were analytically computed from (10), which means to say that the embedding coordinates are of the

form (2). For numerical aspects of derivative estimation from data we refer the reader to Ref. [20].

Although the sampling time does not play any critical role in the following numerical analysis, in order to guarantee a certain uniformity of treatment in the various examples, the sampling time was chosen based on a linear plus nonlinear correlation approach originally suggested in Ref. [21] in such a way as to have the first minimum of the (either linear or nonlinear) correlation function at $\tau \approx 20$. In the present example, that results in decimating the data (x , y and z) with a factor of 7. The decimated data is the working data. Other nonlinear functions which could prove helpful in this type of analysis have been recently put forward in Ref. [22].

The next step is to embed the trajectory in the space (y, \dot{y}, \ddot{y}) , that is the y variable was chosen as the observable, i.e., $s(t) = y(t)$. Reference vectors—working points on the trajectory in the reconstructed space—were chosen by taking 10% of the data of the reconstructed trajectory. Such points were taken uniformly in time. After defining (more on this later) neighborhood size ϵ , a neighbor matrix X_U [see Eq. (8)] was built for each reference vector. Each of the matrices X_U was then decomposed using SVD [see Eq. (9)] using the `svd.m` function of Matlab. Taking the largest singular value of X_U , which is the first element of Σ that is $\sigma_1 = \Sigma(1, 1)$, the statistic in (6) was computed for each of the matrices X_U . It should be clear that each $\sigma_{1\%}$ is a *local* measure of the geometrical structure of the reconstructed space around the corresponding reference vector.

Figure 1 shows $\sigma_{1\%}$ computed for 150 sequential neighborhoods on a trajectory on the Rössler attractor as described. The larger values indicate a more simple local geometry. As the neighborhoods were taken at fixed time intervals along a trajectory on the attractor, the recurrent property is clearly indicated by the regular fluctuations of $\sigma_{1\%}$ along the reference vectors which are uniformly spaced in time (Fig. 1). Moreover, the sharp peaks which reach out to lower values indicate that

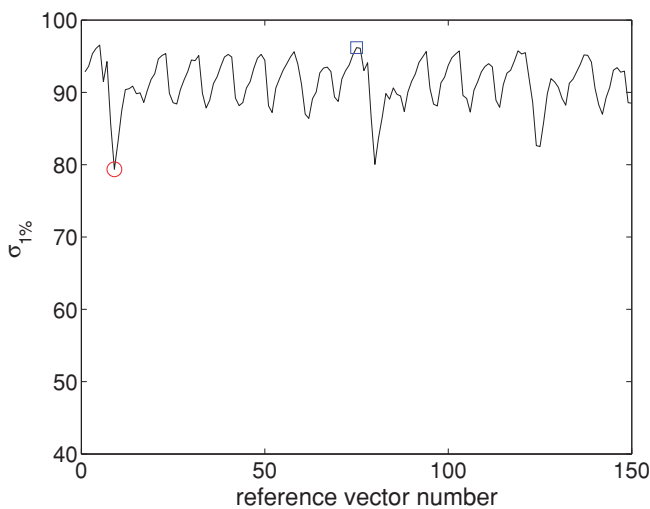


FIG. 1. (Color online) $\sigma_{1\%}$ for 150 sequential neighborhoods on a trajectory on the Rössler attractor reconstructed from the y variable. The ninth reference vector is indicated with a (red) circle and the 75th reference vector is indicated with a (blue) square. For the interpretation of $\sigma_{1\%}$ see text and the caption to Fig. 2.

the system visits regions in the reconstructed space where the local geometry of the attractor is more complicated.

In order to help interpret $\sigma_{1\%}$ further, we choose two extreme values. The one corresponding to the 75th reference vector (a high value) and that corresponding to the ninth neighborhood (a lower value). Each reference vector defines a neighborhood, which is composed of all vectors in the data which are at maximum distance ϵ from the respective reference vector. A few neighbor vectors to each of the 75th and ninth reference vectors are indicated in Fig. 2 (see the caption) and represent simpler and more complex local geometry, respectively. In fact, it can be seen that the vectors in the neighborhood of reference vector 9 are in a region where pleating is more significant. Nonetheless, on the whole, the Rössler attractor represented in the reconstruction space (y, \dot{y}, \ddot{y}) is still quite well unpleated, as indicated by the quite large value of $\sigma_{1\%}$ for all neighborhoods.

A parameter that must be chosen by the user is the tolerance ϵ which defines the neighborhood size. This was varied, for each observable, within the range $1\% \Delta_s \leq \epsilon_s \leq 15\% \Delta_s$, $\Delta_s = \max(s) - \min(s)$, as shown in Fig. 3(a).

From the results reported in Fig. 3(a) it is seen that for almost all neighborhoods the observables are ordered as $y \triangleright x \triangleright z$, indicating that y provides a better quality reconstruction space, according to (7). For neighborhoods that are too small, it becomes difficult to see the difference between x and y . Further simulation studies have shown that the order $y \triangleright x \triangleright z$ in the case of the Rössler system is maintained over a very wide range of neighborhood sizes [Fig. 3(a)] and of sampling times [Fig. 3(b)].

In this and all the remaining examples, the SVDO measures will be numerically reported for $\epsilon_s = 10\%$. Therefore, the values used for the Rössler system were $\epsilon_x = 0.854$, $\epsilon_y = 0.770$, and $\epsilon_z = 0.572$. The values of (7) obtained in this example were $S_x = 0.24$, $S_y = 0.29$, and $S_z = 0.07$. These values are reported in Table I with the order of observability

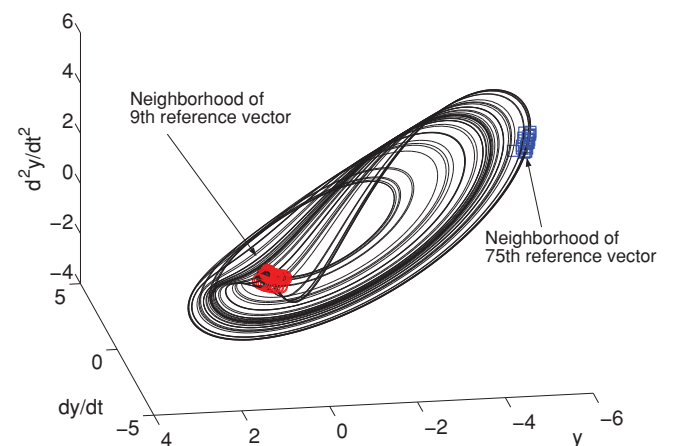


FIG. 2. (Color online) Rössler attractor reconstructed in a differential embedding using the y variable. The (blue) squares are in a neighborhood, of the 75th reference vector, with a high value of $\sigma_{1\%}$ (see Fig. 1), indicating a simple local structure. On the other hand, the (red) circles, where pleating is greater, are in a neighborhood of the ninth reference vector. Such a neighborhood has a low value of $\sigma_{1\%}$ (see Fig. 1), indicating more complex local structure.

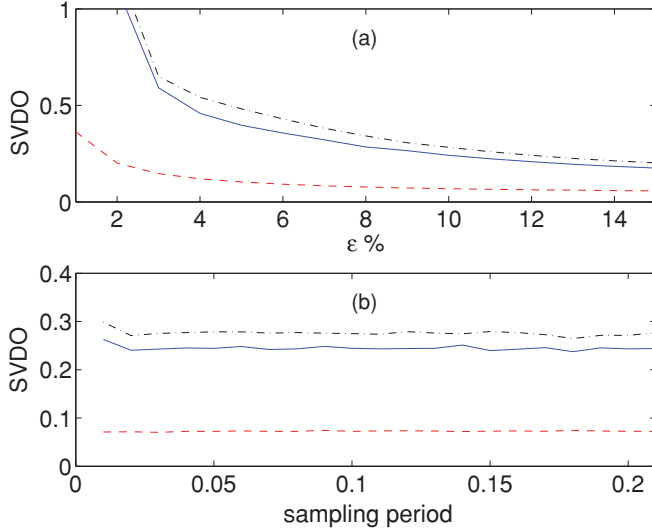


FIG. 3. (Color online) (a) Indices SVDO for the Rössler system for the range $1\% \Delta_s \leq \epsilon_s \leq 15\% \Delta_s$, in this example $\Delta_x = 8.54$, $\Delta_y = 7.70$, and $\Delta_z = 5.72$. (— blue) x , (--- black) y , and (- - - red) z . The sampling time is fixed ($7 \times 0.01 = 0.07$). (b) Same as (a) but with the neighborhood size fixed ($\epsilon = 10\%$) and varying sampling time.

determined using the symbolic computation as defined in Ref. [2]. The results of this example suggest that (7) can be used as an indication of the observability, especially in the case of differential embeddings. For delay coordinates, other parameters such as the delay time and the embedding dimension (and for real data the noise) will play important

TABLE I. The column “observability order” was determined using the symbolic observability coefficients defined in Ref. [2]. The SVDO statistic S_s was computed using Eq. (7) with *differential* coordinates over 100 Monte Carlo runs and noise-free data. In each run the initial conditions of the simulated systems were taken randomly. The observability order for the first three systems was reported in Ref. [25]. The remaining results are reported here.

System	Observability order	s	S_s
Rössler		y	0.29 ± 0.02
	$y \triangleright x \triangleright z$	$\log_{10} z$	0.25 ± 0.03
		x	0.24 ± 0.01
		z	0.07 ± 0.002
Lorenz		z	2.23 ± 0.13
	$z \triangleright x \triangleright y$	x	0.96 ± 0.38
		y	0.43 ± 0.09
Double scroll		x	0.75 ± 0.22
	$x \triangleright z \triangleright y$	z	0.37 ± 0.08
		y	0.54 ± 0.14
Lorenz’84		x	0.44 ± 0.03
	$x \triangleright y \approx z$	y	0.25 ± 0.02
		z	0.18 ± 0.02
Cord attractor		x	0.20 ± 0.04
	$x \triangleright y \approx z$	y	0.05 ± 0.003
		z	0.13 ± 0.01

roles besides the choice of observables. In what follows, we still use differential embeddings so to be able to directly relate (7) with observability properties.

To conclude this example an interesting case will be investigated. It is known that for the Rössler system, if the embedding space is reconstructed with $\log_{10} z$ instead of z , the quality of the resulting space is increased [23]. In other words, $\log_{10} z$ is a better observable than z . If the Rössler system is embedded in the space (s, \dot{s}, \ddot{s}) , where $s = \log_{10} z$ ($\Delta_{\log z} = 1.33$), computation of (7) yields $S_s = 0.25$ (Table I), indicating a clear increase in the quality of the embedding, as compared to the space (z, \dot{z}, \ddot{z}) .

B. A modified model

In order to further illustrate the property of statistic (7) we use the system

$$\begin{aligned} \dot{x} &= -y - z - ax + aF, \\ \dot{y} &= xy - bxz - y + G, \\ \dot{z} &= bxy + xz - z, \end{aligned} \quad (11)$$

with $(a, b, F, G) = (0.25, 4.0, 8.0, 1.0)$, which is a modification of the Lorenz’84 system [24], to be considered in Sec. IV. For these parameter values the system settles to an attractor that has very different features, depending on the region in phase space, as can be seen in Fig. 4. At the center of the figure, the trajectory is squeezed into a very compact region which resembles a cord. On the other hand, apart from the “cord” the attractor displays quite simple *local* dynamics, especially at the center *behind* the “cord.”

Looking at Fig. 1, for the Rössler system, it is seen that the smallest values of $\sigma_{1\%}$ are $\sim 80\%$. The (red) triangles in Fig. 5, for system (11), correspond to $\sigma_{1\%} \approx 80\%$ and are the reference vectors 46 and 70. The reference vectors between the

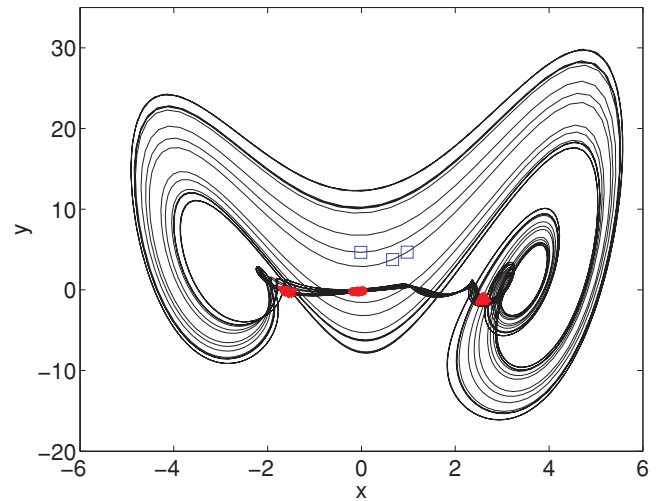


FIG. 4. (Color online) Bidimensional projection of the attractor of system (11), with $(a, b, F, G) = (0.25, 4.0, 8.0, 1.0)$. In the center of the figure the trajectories are squeezed into a very thin region in state space. The (blue) squares at the back of the attractor are some neighbors of reference vector 36 for which $\sigma_{1\%}$ is large. The (red) circles in the center of the cord are neighbors of reference vector 51 for which $\sigma_{1\%}$ reaches one of the smallest values in Fig. 5.

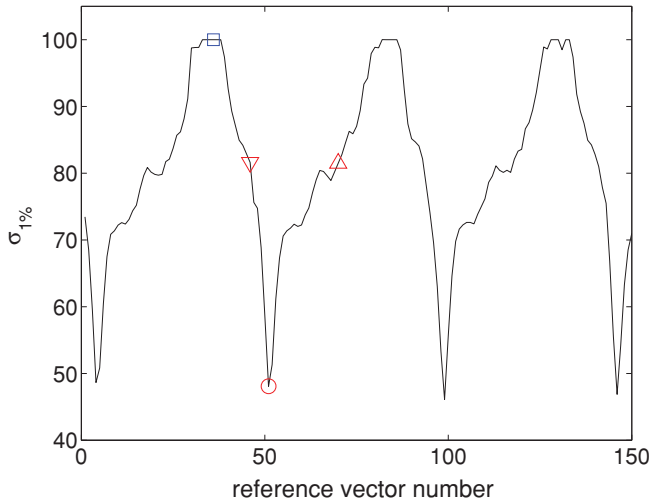


FIG. 5. (Color online) $\sigma_{1\%}$ for 150 sequential neighborhoods on a trajectory on the attractor of (11), with $(a, b, F, G) = (0.25, 4.0, 8.0, 1.0)$.

46th and the 70th are all on the cord and, in fact, correspond to the lowest values of $\sigma_{1\%}$ shown in Fig. 5. The neighbors of the reference vectors 46 and 70 are shown in Fig. 4 as (red) triangles and as the figure clearly shows such neighbors are located at the extremities of the cord. The 51st reference vector, shown as a (red) circle, defines a neighborhood for which $\sigma_{1\%}$ is among the smallest values in Fig. 5, just below 50%. As seen in Fig. 4, such a reference vector is located at a point on the cord where the trajectory is very strongly squeezed. Finally, the reference vector number 36, shown as a (blue) square in Fig. 5, has a high value indicating a very simple local structure in phase space, as is the case behind the cord, where some neighbor vectors of the 36th reference vector are indicated in Fig. 4. Therefore, $\sigma_{1\%}$ serves as a local measure of complexity in phase space.

IV. NUMERICAL RESULTS

Since (7) is, to some extent, a measure of the quality of a reconstructed space, and remembering that the quality of such a space is clearly influenced by the observable (among other important factors), an interesting point to investigate is to see how the observable influences the SVDO statistic. Further, we would like to know to what extent does such a statistic correlate with the observability order for some standard systems.

A. Differential embeddings

Table I shows the results obtained for five different systems. The observability order—obtained from the observability coefficient provided in Ref. [25] and the cited references—is reported with values of S_s .

The other systems investigated and the parameters used are the Lorenz system [26],

$$\begin{aligned}\dot{x} &= \sigma y - \sigma x, \\ \dot{y} &= \rho x - y - xz, \\ \dot{z} &= -\beta z + xy,\end{aligned}\quad (12)$$

with $(\sigma, \rho, \beta) = (10.0, 28.0, 8/3)$. This is an important system to investigate because of the rotation symmetry. As a consequence, two different points, one on each of the attractor wings, cannot be distinguished by looking at z . Unfortunately, this is not revealed by any local measure on the attractor, as discussed in Ref. [27]. Therefore, it comes as no surprise that the values estimated for S_s from each observable taken at a time is consistent with the observability order $z \triangleright x \triangleright y$ obtained in Ref. [25].

The double-scroll attractor is produced by the system [28]

$$\begin{aligned}\dot{x} &= \alpha(y - x - f(x)), \\ \dot{y} &= x - y + z \\ \dot{z} &= -\beta y - \gamma z,\end{aligned}\quad (13)$$

with $f(x) = bx + 0.5(a - b)(|x + 1| - |x - 1|)$ with $a = -8/7$, $b = -5/7$, and $(\alpha, \beta, \gamma) = (9, 100/7, 0)$. The set of equations (13) was integrated with step $\delta_t = 0.05$ from the initial condition $(x_0, y_0, z_0) = (0.1, 0.1, 0.1)$. This system is *locally* linear almost everywhere, and we would expect to have a “global” diffeomorphism almost everywhere, too. The poorer observability properties of the observable y have been felt in the context of data sampling [21], modeling [29], and topological analysis, and the reason is that, because of symmetry, the system’s three fixed points are not distinguishable [30]. The difficulty of assessing the observability features of symmetrical systems using local information has been discussed in Ref. [27]. Although the best observable x is found using SVDO, there is an inversion among the other two variables. This scenario is corrected when delay coordinates are used (see Sec. IV B).

A more challenging case is provided by the Lorenz’84 system [24],

$$\begin{aligned}\dot{x} &= -y^2 - z^2 - ax + aF, \\ \dot{y} &= xy - bxz - y + G, \\ \dot{z} &= bxy + xz - z,\end{aligned}\quad (14)$$

with $(a, b, F, G) = (0.25, 4.0, 8.0, 1.0)$. This system settles to a chaotic attractor that results from a torus breakdown, which is less homogeneous than the previous ones considered so far. The observability order arrived at using the definitions based on Lie derivatives [1] and the symbolic coefficients defined in Ref. [2] was $x \triangleright y \approx z$. The SVDO statistic for this system clearly indicates x as the variable that provides the best local average unpleating of the dynamics and places y slightly ahead of z , as indicated in Table I.

To close this section we return to the modified model (11). Figure 6(a) shows a three-dimensional view of the attractor. It is interesting to notice that the cord is basically parallel to the direction of the x coordinate, as confirmed by a two-dimensional (2D) projection on the y - z plane, Fig. 6(b). That means that x is necessarily an important observable because if it is not used, the cord is practically not seen at all, as can be gathered from Fig. 6(b).

In fact, this property, which can be pictorially appreciated in Fig. 6, can also be quantified. Using the observability coefficients δ_s defined in Ref. [1], we find $\delta_x = 0.0104$, $\delta_y = 0.0005$, and $\delta_z = 0.0005$, which indicate the observability order $x \triangleright y \approx z$. Computing the SVDO statistic proposed

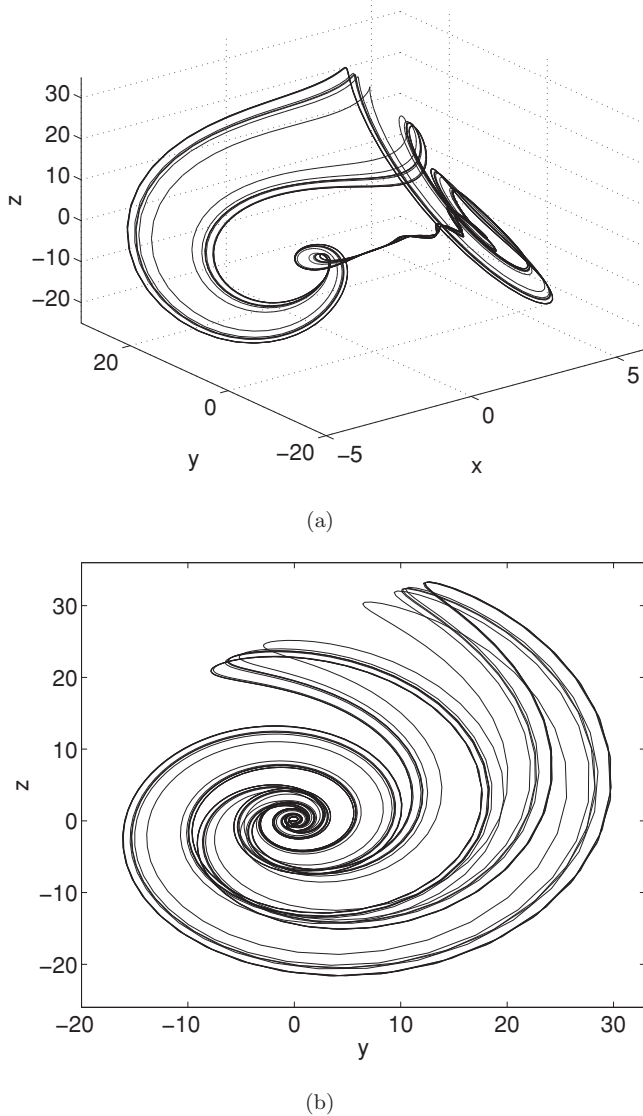


FIG. 6. (a) A 3D view of the “cord attractor” of system (11), and (b) $y \times z$ plane projection. If the x variable is not recorded, the cord part of the attractor cannot be seen.

in this paper the following results are found (see Table I): $S_x = 0.20$, $S_y = 0.05$, and $S_z = 0.13$. These numbers confirm that a better reconstruction was obtained from the x variable, which is due mainly to the fact that x is a better observable. The SVDO indices also suggest that in the differential space reconstructed from the z variable, there is less variability in the complexity of the local geometry—better unpleating of the dynamics—than from the y variable, although, from a theoretical point of view, y and z are basically equivalent.

In general, SVDO does correlate generally well with observability results, although such a statistic will also take other aspects (not only observability) into account. However, this feature is offset by the significant advantage that *no equations are required* to compute SVDO. Up to here, to avoid possible numerical artifacts due to the estimation of derivatives, the known vector field was used to obtain \dot{s} and \ddot{s} .

In the following section, the quality of the delay embeddings is assessed only from data.

B. Delay embeddings

The results in this section were obtained starting from data embedded in delay coordinates. As the main concern is *not* to define embedding parameters, the results have been obtained with such parameters taken from the literature, whenever available. The standard Rössler system was simulated for other values of the embedding dimension (above the minimum dimension), and for the time delay and the results remain qualitatively the same. Therefore, the results to be presented do not depend critically on either d or τ , as long as d is greater or equal to the minimal value needed for an embedding. The study includes the investigation of additive noise. In each case, after simulation of the system and recording of the variable s , the working data were obtained by adding to s white Gaussian noise e . Four noise levels were simulated: noise-free, 1%, 5%, and 10%. The noise percentage is defined as $\text{std}(e)/\text{std}(s) \times 100$. The simulations were carried out in a Monte Carlo fashion, over 100 runs, where initial conditions and noise realizations were randomly taken for each run. The results obtained are shown in Table II.

The embedding parameters used for the Rössler system were obtained in Ref. [31], namely, $d = 4$ and $\tau = 1.54$. The delay time was chosen in that reference equal to 1/4 of the pseudoperiod. This will be maintained in all examples. The embedding parameters for the Lorenz attractor were $d = 4$ and $\tau = 0.13$ [16]. The double scroll was embedded with $d = 4$ and $\tau = 0.5$, according to Ref. [32]. Embedding parameters of the Lorenz’84 model were $d = 5$ and $\tau = 0.86$, as indicated in Ref. [33]. For this last system with 10% noise the size of the neighborhood was increased to $\epsilon = 15\%$ in order to guarantee $N > d$ [see just above Eq. (5)].

In analyzing the results shown in Table II, it should be noted that even the noise-free results can only be compared to those in Table I in relative terms. In other words, the SVDO statistic helps to compare observables in the *same set of coordinates*. What must be compared is how close the ordering of recorded variables obtained using SVDO comes to the observability order obtained from the analytical observability coefficients. This is, in fact, the main purpose of such coefficients: to assist in the choice of the best observable for investigating a given system. Also, it is important to notice that in none of the simulated examples, the noise altered such ordering.

As for the effects of the noise, the general gradual decrease of the SVDO statistic with noise (with only a few exceptions) is somewhat expected because the noise, locally, blurs the local structure of the reconstructed space. The significant robustness of the results for the different noise levels and the fact that the order of recorded variables indicated by the SVDO statistic did not change with the noise is a welcome feature.

C. Sunspot data

We analyze a standard benchmark set of data, the sunspot data. One of the reasons for choosing these data is that for the underlying dynamics there are two sets of available data, namely, the original and a transformed set. Also, previous

TABLE II. SVDO statistic computed using Eq. (7) and *delay* coordinates over 100 Monte Carlo runs. In each run a different realization of additive noise was used and the initial conditions of the simulated systems were taken randomly. The noise level is given in percentage of the standard deviation with respect to the standard deviation of the noise-free signal. (*) The results for the Lorenz'84 system with 10% noise are reported for $\epsilon = 15\%$, and in all other cases $\epsilon = 10\%$ was used. The column "observability order" was determined using the symbolic observability coefficients defined in Ref. [2].

System	Observability order	s	S_s with percentage noise = $\frac{\text{std}(\epsilon)}{\text{std}(s)} \times 100$			
			0%	1%	5%	10%
Rössler	$y \triangleright x \triangleright z$	x	0.64 ± 0.04	0.64 ± 0.03	0.53 ± 0.04	0.45 ± 0.05
		y	0.64 ± 0.04	0.63 ± 0.04	0.53 ± 0.04	0.46 ± 0.04
		$\log_{10} z$	0.53 ± 0.04	0.52 ± 0.03	0.52 ± 0.03	0.49 ± 0.04
		z	0.21 ± 0.01	0.21 ± 0.01	0.20 ± 0.01	0.19 ± 0.01
Lorenz	$z \triangleright x \triangleright y$	z	1.40 ± 0.11	1.41 ± 0.11	1.28 ± 0.15	1.06 ± 0.10
		x	0.20 ± 0.04	0.19 ± 0.04	0.15 ± 0.03	0.13 ± 0.02
		y	0.13 ± 0.02	0.13 ± 0.02	0.11 ± 0.02	0.09 ± 0.01
Double scroll	$x \triangleright z \triangleright y$	x	0.76 ± 0.16	0.76 ± 0.15	0.74 ± 0.13	0.71 ± 0.08
		z	0.47 ± 0.09	0.48 ± 0.09	0.45 ± 0.01	0.52 ± 0.07
		y	0.40 ± 0.04	0.38 ± 0.05	0.34 ± 0.04	0.31 ± 0.04
Lorenz'84	$x \triangleright y \approx z$	x	0.73 ± 0.06	0.75 ± 0.06	0.79 ± 0.06	$0.51 \pm 0.03^*$
		y	0.53 ± 0.13	0.52 ± 0.11	0.57 ± 0.17	$0.29 \pm 0.04^*$
		z	0.53 ± 0.14	0.55 ± 0.20	0.65 ± 0.29	$0.33 \pm 0.04^*$
Cord attractor	$x \triangleright y \approx z$	x	0.35 ± 0.029	0.34 ± 0.025	0.33 ± 0.028	0.31 ± 0.028
		y	0.04 ± 0.002	0.04 ± 0.002	0.04 ± 0.002	0.04 ± 0.002
		z	0.04 ± 0.002	0.04 ± 0.002	0.04 ± 0.002	0.03 ± 0.001

studies have revealed that the transformed data unpleat the dynamics in a better way, thus providing better observability properties. The brief description of the data sets in Ref. [25] will be helpful.

"The time series composed of sunspot number was built as annual means from 1700 up to 1749, when monthly means started to be used and this went until 1818. It was only from 1818 that daily indices were used to compose the time series. Thus, no more than 23 cycles are available at the moment. The sunspot numbers before 1850 were reconstructed by Wolf [34] and are somewhat unreliable since some characteristics of the underlying dynamics are significantly different for the data recorded before and after 1850 [35], and the data are not of uniform quality [36], thus some authors do not use the first part of the time series [37]. Even after 1850, the dynamics appears to be nonstationary, that is, there is still some change in the dynamics which cannot be explained in terms of a low-dimensional deterministic system [35]. Other authors have preferred using a slightly transformed version of Wolf's data [38] or even to define a new time series based on the daily group sunspot number [39].

"The reversals of the Sun's magnetic field have been introduced using the so-called Bracewell statistic [40]. Such a procedure presents the disadvantage of forcing the trajectory to pass near the origin of the reconstructed space when switching from one cycle to the next [41]. Moreover, in that domain, the noise contamination becomes relatively more significant to the point that successful global modeling becomes very hard. Also, there are topological reasons why the Bracewell index should be avoided [41]. Reversing every other cycle corresponds to locating the rotation axis at the origin of the phase space.

Thus the cover of the phase portrait is made of two separate attractors—each attractor is associated with one specified polarity—and it is not possible to have an inversion of the magnetic polarity at each cycle without breaking the causality chain: this explain why no satisfactory global modeling can be obtained from this index. Moreover, as discussed in the last reference, it is possible (and advantageous) to take into account the symmetry that can be expected in a scenario such as the solar dynamo. In a recent work, methods of computational topology were used to analyze the dynamics of large scale solar magnetic field [42], although earlier attempts to use topological concepts in the understanding and modeling of solar dynamics have been reported [43]. From the modeling point of view, the aforementioned transformation is important because it unpleats the dynamics and therefore it improves modeling [...]. The details of such a transformation have been described in [41] [...]" [44] The time series in the original and transformed spaces are shown in Fig. 7.

In order to compute the SVDO statistic in Eq. (7), the time series had to be embedded. Following Ref. [41] we used $d = 3$ with time delays in the range $10 \leq \tau \leq 20$. Because the time series is not too long (~ 3000 data points) in order to perform Monte Carlo simulation, the reference vectors were taken *randomly* on the attractor, rather than uniformly distributed in time, as before. As in the previous examples, $\epsilon = 10\% \Delta$ and 10% of the embedded vectors were randomly chosen to be reference vectors. This was performed 500 times for each time series shown in Fig. 7. The mean values of the SVDO statistic and the $\pm \sigma$ bands, computed over the 500 Monte Carlo runs, are shown in Fig. 8.

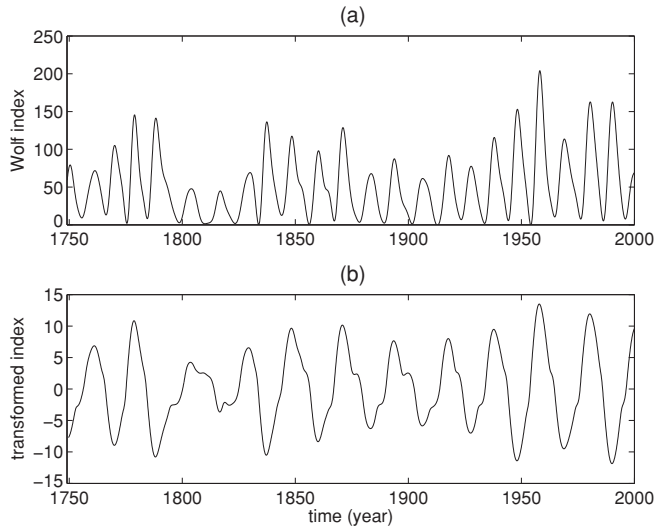


FIG. 7. Sunspot data in (a) the original space, (b) the transformed space. For details on smoothing of the original data and transformation, see Ref. [41].

Two features are immediately clear from Fig. 8. First, the mean value of SVDO is smaller for the time series in the original space than for the counterpart in the transformed space, with the exception of the value computed for $\tau = 19$. Second, the sample standard deviation of SVDO increases with τ . The reason for this is that as the time delay increases, there are less embedded vectors available, that is, some of the local matrices $X_{\mathcal{U}}$ have relatively few vectors. Therefore, numerically, the problem becomes less well behaved for larger values of τ . The same effect would be noticed for larger values of the embedding dimension d .

A good working value for the delay time was considered to be $\tau = 16$ months [41]. For the delay embedding determined by $d = 3$ and $\tau = 16$, the estimated values using Eq. (7) were $S_{\text{original}} = 0.12 \pm 0.06$ and $S_{\text{transformed}} = 0.17 \pm 0.04$. The results in Fig. 8 confirms that, in fact, the transformed time series provides a significantly better observability ($p < 0.01$) of the solar dynamics.

V. CONCLUSION

This paper has put forward a statistic (SVDO) that uses the SVD decomposition of matrices build with *local* data. It has been argued that such a statistic serves as a measure of how homogeneous is the geometry of an attractor throughout space. When the dynamics of the original system are unpleated rather homogeneously in the reconstructed space (from a geometrical point of view), the computed statistic is larger than for spaces where the aforementioned unpleating is not so homogeneous. For instance, if in the reconstructed space there are regions with sharp pleatings or regions where the trajectories are squeezed, the statistic assumes lower values.

The statistic put forward in this paper correlates generally well with the observability order of a given system. This is of great practical importance because it permits to indirectly quantify observability *from a time series*. The use of the

proposed statistic as an indication of the degree of observability is an inference which is based on the assumption that a good

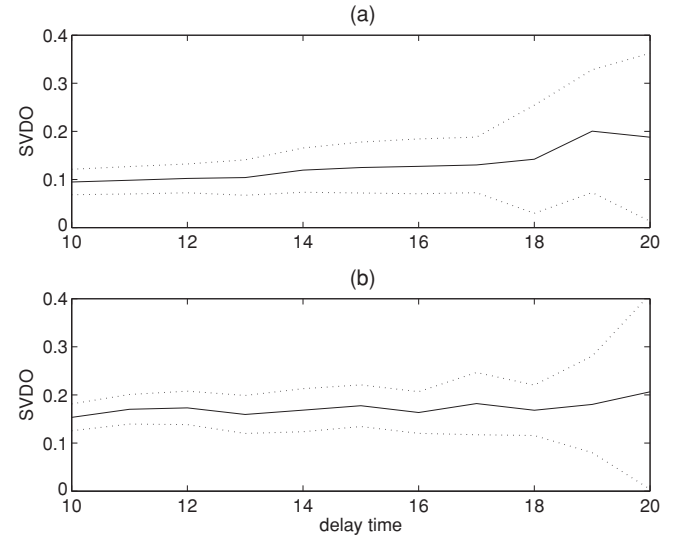


FIG. 8. Statistic SVDO (7) for embedding dimension $d = 3$ and various time delays for sunspot data in (a) the original space, (b) the transformed space. The thick line is the average value of the SVDO statistic over 500 Monte Carlo runs (see text for details) and the confidence bands are \pm one standard deviation.

observable will unpleat the dynamics more homogeneously than a bad observable in a space of sufficiently high dimension. The statistic evaluates the local geometrical complexity by means of a SVD decomposition, and then the global homogeneity of the reconstructed space is quantified using the sample average and sample standard deviation of the local measures.

The SVDO statistic was computed for various standard systems and, as mentioned formerly, it correlates nicely with the observability order. The numerical investigation considered differential and delay embeddings and in the latter case four different noise levels were used. Very few (slight) discrepancies were noticed when compared to results obtained using observability theory (that uses the known equations). Such discrepancies are a fair price to pay for not having to use equations.

The paper also includes an example using the sunspot time series for which there are no theoretical equations for the underlying dynamics. Relying on previous works, the SVDO was computed for the sunspot data in the original space and also for transformed data which are known (from topological and numerical modeling experience) to provide better observability of the sun dynamics. The obtained results were consistent with such knowledge.

ACKNOWLEDGMENTS

This work has been partially supported by CNPq (Brazil) and CNRS (France).

- [1] C. Letellier, L. A. Aguirre, and J. Maquet, *Phys. Rev. E* **71**, 066213 (2005).
- [2] C. Letellier and L. A. Aguirre, *Phys. Rev. E* **79**, 066210 (2009).
- [3] R. Hermann and A. J. Krener, *IEEE Trans. Autom. Control* **22**, 728 (1977).
- [4] D. Smirnov, B. Bezruchko, and Ye. Seleznev, *Phys. Rev. E* **65**, 026205 (2002).
- [5] D. S. Broomhead and G. P. King, *Physica D* **20**, 217 (1986).
- [6] N. H. Packard, J. P. Crutchfield, J. D. Farmer, and R. S. Shaw, *Phys. Rev. Lett.* **45**, 712 (1980).
- [7] F. Takens, *Lect. Notes Math.* **898**, 366 (1981).
- [8] R. Nagarajan, *Int. J. Bifurcation Chaos* **15**, 1515 (2005).
- [9] B. P. Bezruchko and D. A. Smirnov, *Extracting Knowledge From Time Series* (Springer, Berlin, 2010).
- [10] M. Paluš and I. Dvořák, *Physica D* **55**, 221 (1992).
- [11] P. G. Vaidya, P. S. Anand, and N. Nagaraj, *Acta Appl. Math.* **112**, 205 (2010).
- [12] D. S. Broomhead, R. Jones, and G. P. King, *J. Phys. A* **20**, L563 (1987).
- [13] Th. Buzug and G. Pfister, *Phys. Rev. A* **45**, 7073 (1992).
- [14] K. Fukunaga and D. R. Olsen, *IEEE Trans. Comput.* **20**, 176 (1971).
- [15] C. Letellier, L. A. Aguirre, and J. Maquet, *Commun. Nonlinear Sci. Numer. Simul.* **11**, 555 (2005).
- [16] Th. Buzug and G. Pfister, *Physica D* **58**, 127 (1992).
- [17] O. E. Rössler, *Phys. Lett. A* **57**, 397 (1976).
- [18] G. Gouesbet and C. Letellier, *Phys. Rev. E* **49**, 4955 (1994).
- [19] C. Letellier, *Phys. Rev. Lett.* **96**, 254102 (2006).
- [20] C. Letellier, L. A. Aguirre, and U. S. Freitas, *Chaos* **19**, 023103 (2009).
- [21] L. A. Aguirre, *Phys. Lett. A* **203**, 88 (1995).
- [22] Q. M. Zhu, L. F. Zhang, and A. Longden, *Automatica* **43**, 1519 (2007).
- [23] C. A. Ibanez, *Rev. Mex. Fís.* **52**, 64 (2006).
- [24] E. N. Lorenz, *Tellus Ser. A* **36**, 98 (1984).
- [25] L. A. Aguirre, S. B. Bastos, M. A. Alves, and C. Letellier, *Chaos* **18**, 013123 (2008).
- [26] E. N. Lorenz, *J. Atmos. Sci.* **20**, 130 (1963).
- [27] C. Letellier and L. A. Aguirre, *Chaos* **12**, 549 (2002).
- [28] L. O. Chua, M. Komuro, and T. Matsumoto, *IEEE Trans. Circuits Syst.* **33**, 1072 (1986).
- [29] L. A. Aguirre, G. G. Rodrigues, and E. M. A. M. Mendes, *Int. J. Bifurcation Chaos* **7**, 1411 (1997).
- [30] C. Letellier, G. Gouesbet, and N. F. Rulkov, *Int. J. Bifurcation Chaos* **6**, 2531 (1996).
- [31] M. Small and C. K. Tse, *Physica D* **194**, 283 (2004).
- [32] U. Parlitz, *J. Circ. Syst. Comput.* **3**, 507 (1993).
- [33] M. B. Kennel and S. Isabelle, *Phys. Rev. A* **46**, 3111 (1992).
- [34] R. Wolf, *C. R. Acad. Sci. (Paris)* **35**, 704 (1852).
- [35] M. Carbonell, R. Oliver, and J. L. Ballester, *Astron. Astrophys.* **290**, 983 (1994).
- [36] J. A. Eddy, *Science* **192**, 1189 (1976).
- [37] A. Orfila, J. L. Ballester, R. Oliver, A. Alvarez, and J. Tintoré, *Astron. Astrophys.* **386**, 313 (2002).
- [38] Q. X. Li and K. J. Li, *Chin. J. Astron. Astrophys.* **7**, 435 (2007).
- [39] D. V. Hoyt and K. H. Schatten, *Sol. Phys.* **179**, 189 (1998).
- [40] R. N. Bracewell, *Nature (London)* **171**, 649 (1953).
- [41] C. Letellier, L. A. Aguirre, J. Maquet, and R. Gilmore, *Astron. Astrophys.* **449**, 379 (2006).
- [42] N. G. Makarenko, L. M. Karimova, and M. M. Novak, *Physica A* **380**, 98 (2007).
- [43] M. N. Kremliovsky, *Sol. Phys.* **151**, 351 (1994).
- [44] Also, the transformed data are available at [<http://www.atomosyd.net>].